# COVER SHEET

Strange, Andrew and Ralston, Jonathon and Chandran, Vinod (2005) Near-Surface Interface Detection for Coal Mining Applications Using Bispectral Features and GPR. *Subsurface Sensing Technologies and Applications* 6(2):pp. 125-149.

# Near-Surface Interface Detection for Coal Mining Applications Using Bispectral Features and GPR

*Andrew D. Strange, Jonathon C. Ralston*, Vinod Chandran*

Image and Video Research Lab, Queensland University of Technology,
2 George Street, Brisbane, Q 4001, Australia
a.strange@qut.edu.au

* CSIRO, Exploration & Mining, 1 Technology Court, Pullenvale, Q 4069, Australia

## ABSTRACT

The use of ground penetrating radar (GPR) for detecting the presence of near-surface interfaces is a scenario of special interest to the underground coal mining industry. The problem is difficult to solve in practice because the radar echo from the near-surface interface is often dominated by unwanted components such as antenna crosstalk and ringing, ground-bounce effects, clutter, and severe attenuation. These nuisance components are also highly sensitive to subtle variations in ground conditions, rendering the application of standard signal pre-processing techniques such as background subtraction largely ineffective in the unsupervised case. As a solution to this detection problem, we develop a novel pattern recognition-based algorithm which utilizes a neural network to classify features derived from the bispectrum of 1D early time radar data. The binary classifier is used to decide between two key cases, namely whether an interface is within, for example, 5 cm of the surface or not. This go/no-go detection capability is highly valuable for underground coal mining operations, such as longwall mining, where the need to leave a remnant coal section is essential for geological stability. The classifier was trained and tested using real GPR data with ground truth measurements. The real data was acquired from a testbed with coal-clay, coal-shale and shale-clay interfaces, which represents a test mine site. We show that, unlike traditional second order correlation based methods such as matched filtering which can fail even in known conditions, the new method reliably allows the detection of interfaces using GPR to be applied in the near-surface region. In this work, we are not addressing the problem of depth estimation, rather confining ourselves to detecting an interface within a particular depth range.

## KEY WORDS

GPR, bispectrum, interface detection, horizon control, coal mining.

## TITLE AFILIATIONS

Andrew D. Strange & Vinod Chandran
Image and Video Research Lab, Queensland University of Technology, 2 George Street, Brisbane, Q 4001, Australia,
Email: andrew.strange@nbc.org.au

Jonathon C. Ralston
CSIRO, Exploration & Mining, 1 Technology Court, Pullenvale, Q 4069, Australia

## 1. Introduction

One of the current challenges with automating underground coal mining machinery is measuring and maintaining a coal mining horizon [1]. The coal mining horizon is the horizontal path the machinery follows through the undulating coal seam during the mining operation. A thin layer of low quality coal is typically found between the actual coal seam and surrounding clay layers [2]. A typical mining practice is to leave a thin remnant of high-quality coal unmined in order to maintain geological stability of the cutting face. If the remnant layer is too thick, resources are wasted as the unmined coal is permanently unrecoverable. If the remnant layer is too thin, the product is diluted and there is an increased risk of roof fall. The challenge therefore is to develop a sensing method to detect the interface between the high quality coal and low quality coal layers which can be integrated into an automatic horizon control system. If the interface is within a predetermined depth of the coal surface (coal thickness is less than a set threshold), the optimal amount of extracted coal has been reached and the mining machine should retreat. If the interface is not within the specified depth, more coal can be extracted. The overall benefits are improved coal quality, increased mining productivity and enhanced worker safety [3].

There are two categories of sensors in underground coal mining for horizon control – reactive and predictive. Reactive sensors are based on detecting changes in the mining operational characteristics when the interface separating the coal and surrounding strata is encountered. The reactive sensors are limited as the miner has already cut into the low quality coal and surrounding strata when the interface is detected which damages the machinery and dilutes the coal. Some examples of reactive sensors are monitoring cutting drum current, sensing changes in machine vibration signatures and instrumented cutting picks [3]. Predictive approaches however sense the remnant coal thickness before it is mined and thus allow for optimal mining. The most common predictive technique uses a natural gamma radiation sensor to estimate the coal thickness by exploiting the radioactivity of host strata found with many coal deposits. The efficacy of this technique is highly site specific as well as requiring long processing delays (up to 30 seconds) to obtain a reliable depth estimate [3]. This time delay can impact significantly coal mining production rates. More recent claims by Stolarczyk and Stolarczyk [2] indicate the development of a sensor that can estimate coal thickness from the real and imaginary impedance of a resonant microstrip patch antenna. This system has been commercialized and installed on a continuous miner in Carlinville, Illinois, USA [4]. However, to the authors' knowledge, a qualitative analysis of this system and the sensor thickness estimation range are yet to be published. A promising alternative to the limitations of these predictive approaches in this seam detection application is the use of ground penetrating radar (GPR) [1].

GPR is a non-invasive technique used to obtain information about media beneath the earth's surface. In impulse GPR systems, a short pulse of electromagnetic energy is transmitted into the ground. A proportion of this energy is reflected back towards the surface at interfaces of media with differing electromagnetic properties. Information about the sub-surface can be extracted from the amplitude and time delay of these reflections. There are many applications that use GPR for sub-surface detection tasks such as archaeology, pipe and cable detection, geological profiling, buried landmine detection [5], snow thickness estimation and pavement evaluation [6].

Some research using GPR for coal seam thickness detection and/or estimation have been previously undertaken. Ellerbruch and Belsher [7] developed an FM-CW GPR to measure coal layer thickness. They achieved reasonable results although the desired accuracy was not achieved to warrant further research [8]. Daniels [9] investigated the feasibility of coal seam thickness estimation with short pulse GPR, concluding that it was feasible to use GPR for this task however more sophisticated signal processing techniques were required. Chufo [10] developed a stepped-frequency radar coal thickness sensor in which the antenna module is moved through 32 positions to obtain one thickness estimate. This system is unsuitable for use as a horizon control sensor as it is not a real-time solution and the antenna module would not survive the harsh mining environment. Noon [8] developed a prototype stepped-frequency GPR with resolving power better than 8 cm primarily for high resolution mapping of thin coal seams for open cut coal mining. Mowrey et al. [11] used GPR to monitor coal-rib thickness in highwall mining. The 500 MHz centre frequency system was found to measure rib thickness from 0.9 m to more than 3 m. This range does not include the near-surface interface depth as required for horizon control sensing. Yelf [12] demonstrated the capability of GPR to monitor changes in the interface to assist operators in machine guidance. Jha et al. [13] used stepped frequency GPR to map barrier thickness in coal mines. Ralston and Hainsworth [1,3] investigated coal seam thickness estimation using impulse GPR with promising results. Preliminary research has shown that using GPR as a horizon control sensor is possible and the key to the final solution is real-time intelligent data processing [14]. One implementation restraint that must be considered is the antennas must be ground-coupled as the operating environment for the horizon control sensor is very extreme [15].

There are two general target structures in subsurface imaging, namely isolated objects and interfaces of layered media. When data is acquired in the form of a B scan (received traces displayed vertically as the GPR traverses a horizontal distance), the GPR signature for isolated objects assumes the form of a diffraction hyperbola. An example of an isolated object is the buried landmine. For layered media, the interfaces appear as bands across the images. In the horizon control sensor context, the targets are interfaces. The general structure for imaging a coal mine with GPR is shown in Figure 1.

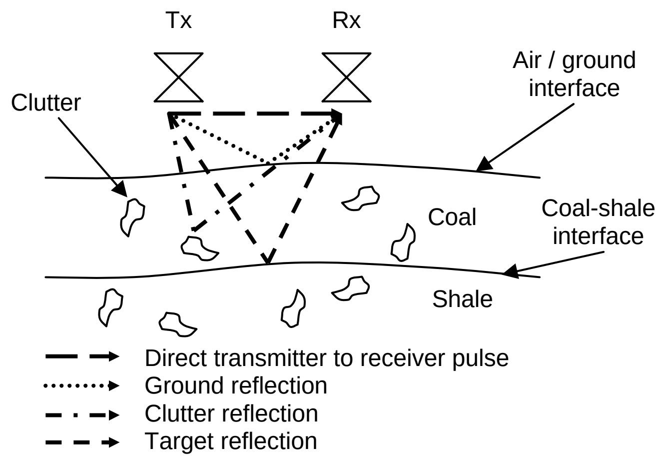


**Figure 1.** GPR deployment to scan layered media below the earth's surface. The electromagnetic pulses are transmitted and received by two antennas of dimension proportional to the desired wavelength of investigation.

This paper presents a pattern recognition approach using features based on the bispectrum to detect the presence of an interface close to the surface. This detection method has previously shown very promising results with synthetic data in [16], but lacked real-data validation. To this end, a testbed with coal-shale, coal-clay and shale-clay interfaces has been constructed and ground truth data obtained for comparison with this detection method.

## 2. GPR Signal Processing for Seam Detection

This section presents details on the processing method used for detecting the seam boundary. It highlights some of the key limitations associated with the application of classic processing techniques to this problem, which serve to provide a strong motivation for employing emergent pattern recognition techniques.

### 2.1 Classical Approaches

In some ways, the near-surface interface detection scenario is similar to that encountered in pavement evaluation and so it is useful to briefly review the practical efficacy of GPR-based sensing technology for this task. The use of GPR for pavement evaluation has been well documented [17-20] and is a well established technique. Current techniques for this application were quantitatively tested with both asphalt and concrete pavements. Asphalt pavement thickness can be reliably estimated over the range 50 to 200 mm with an accuracy of 2.5 mm with site calibration [17]. This method uses a GPR system with bistatic air-coupled horn antennas mounted to the back of a vehicle. The systems can acquire data at a rate such that the vehicle can travel at highway speeds scanning the pavement without the need for lane closure. Information about the pavement can be obtained from the peak amplitude and time delay of reflected echoes, or by the use of the matched filter [18,19].

In contrast to asphalt pavement which typically has low conductivity, concrete pavement is lossy due to the water content [17]. As a result of the signal attenuation from propagating through a lossy medium, the air-coupled GPR system for asphalt evaluation is unable to estimate concrete thickness. This led to the investigation of ground-coupled antenna systems. In this configuration, the antennas are in direct contact with the surface which allows more energy to propagate into the ground. There are two techniques in which ground-coupled antennas are used. The more common for qualitative real-time mapping is when the transmitter and receiver antennas are in the fixed-offset bi-static configuration. Maser reported in [17] that the accuracy of thickness estimates obtained with the fixed-offset ground-coupled antennas is not satisfactory for either asphalt or concrete pavement evaluation. This is primarily due to the uncertainty in the wave propagation velocity estimate of the top layer. Another ground-coupled method investigated by Maser was the common midpoint (CMP) which has shown reasonable results for estimating concrete pavement thickness. Unfortunately CMP cannot be used to acquire data at highway speeds as the antenna separation needs to be progressively increased between scans while scanning the same point.

Other popular processing techniques involve forward and inverse modeling based on physical models and approximate numerical solutions to Maxwell's equations [21,22]. Although these methods have shown good results at characterizing the subsurface, they can be difficult to apply to different imaging scenarios and can be computationally intensive. The simplifying assumption of far-field propagation in [21] would not be valid for the GPR horizon control sensor due to the ground-coupled antenna requirement.

Other near-surface processing schemes typically suppress ground clutter as a pre-processing tool for detecting landmines [23-27]. Ebihara [28] used blind separation and time-frequency signal processing to suppress ground clutter in data acquired with a 100 MHz GPR system during the investigation of a permafrost layer 1 metre below the ground surface. Even though successful results were reported, the interface depth range for the horizon control sensor is significantly lower.

In summary, there are important lessons to be learned from the pavement analysis scenario and other classical processing techniques. Air-coupled horn antennas would be susceptible to damage from the hazardous underground coal mine environment. The real-time requirement means that CMP is not suitable as the delays encountered during data acquisition will limit production. For the same reason, techniques based on inversion and optimization are impractical for a real-life mining scenario.

### 2.2 Matched Filter

The objective of the matched filter is to recognize the presence of a known deterministic signal in additive Gaussian noise [29]. The filter correlates the received waveform with a reversed time shifted version of the transmitted signal. In practice, the transmitted signal is estimated from windowing the reflection of a flat metal plate and is usually acquired when calibrating the GPR system [19]. To detect the signal component of a discrete-time sequence $x(n)$, the likelihood ratio function is computed using

$$L(n) = \exp\left\{ -\frac{1}{2\sigma^2}\left( \sum_{m=0}^{M-1} s^2(m) - 2\sum_{m=0}^{M-1} x(n-m)s(m) \right) \right\} \tag{1}$$

where $n$ is the sample number, $s(n)$ is the estimate of the transmitted signal with length $M$, $x(n)$ is the received signal and $\sigma^2$ is the noise variance (average noise power). The peak time of the likelihood ratio function can be used as a time delay estimate of the target reflection. The depth of the target can then be estimated from the time delay estimate using

$$d = vn\Delta t \tag{2}$$

where $v$ is the electromagnetic wave propagation velocity, $\Delta t$ is the sampling period and $n$ is the sample number of the likelihood ratio function peak. The wave propagation velocity can be obtained from measuring the travel time through a layer of known thickness or using

$$v = \frac{c}{\sqrt{\varepsilon_r}} \tag{3}$$

where $c$ is the electromagnetic wave propagation velocity in free space and $\varepsilon_r$ is the real relative permittivity. The upper layer relative permittivity can be estimated from the flat metal plate scan with air-coupled antennas as described in [17] and [20], published values or by taking measurements with dielectric measuring equipment.

The limiting factor with using the matched filter is the lower resolution limit. For the case when the antennas are air-coupled, the near-surface target reflection can be masked by the ground reflection. If the antennas are ground-coupled, the near-surface target reflection is masked by the direct transmitter to receiver component and antenna ringing. A common technique to solve this problem is the subtraction of the mean trace. This can give satisfactory results when imaging isolated objects, however the response from an interface is filtered out using this process.

Therefore the classical techniques mentioned above are deemed unsuitable for the radar based horizon control sensor.

### 2.3 Other Pattern Recognition Approaches

The important practical problems associated with the use of classical analysis methods strongly motivate the investigation into alternate processing techniques for the coal seam horizon sensing task. To this end we propose the use of pattern recognition techniques for this problem. Pattern recognition is the act of taking raw data and making an action based on the *category* of the pattern [30]. There are celebrated cases where pattern recognition has been applied to GPR processing tasks. Chan et al. [31] modeled backscattered echoes as a linear combination of exponentially damped sinusoid functions to identify buried plastic targets. Carevic et al. [32,33] used similar features to classify buried landmines. Al-Nuaimy et al. [34] used features derived from the power spectrum for underground pipe detection.

Neural networks, which are frequently used for a range of pattern detection and classification tasks, have also been used for various GPR processing problems. Some applications include detecting the presence of hyperbolic signatures in GPR images for underground pipe detection [34-36], interpretation of GPR images of reinforced concrete [37] and buried landmine detection [38,39]. In some cases, the data as either A scans (received signal displayed horizontally) or B scans with limited pre-processing is fed directly into the neural network classifier. The alternative is to extract features from the data which are then used as the neural network inputs. The key to satisfactory results using pattern recognition approaches is to use features whose clusters provide discrimination between different classes. The features and classifier employed in this work are discussed in the following sections.

### 2.4 Power Spectrum

The power spectrum has been used as a feature vector with a neural network classifier to detect pipes and landmines [34]. The power spectrum can be estimated with the periodogram [40]. The periodogram of a band-limited finite-duration discrete-time sequence is computed as

$$S_X(f) = \frac{1}{LU}\left|\sum_{n=0}^{L-1} w(n)x(n)e^{-j2\pi fn}\right|^2 \tag{4}$$

where *w(n)* is a rectangular window, *L* is the finite-length segment of *x(n)* and *U* is a normalization factor calculated using

$$U = \frac{1}{L}\sum_{n=0}^{L-1}[w(n)]^2 \ . \tag{5}$$

If *w(n)* is not a rectangular window, equation (4) becomes the modified periodogram. Other power spectrum estimation tools such as the Welch averaged periodogram are useful for detecting periodic signals in additive noise [40]. Most GPR systems have relatively high scanning output rates and so obtaining multiple realizations for averaging is easy if required.

### 2.5 Bispectral Features

We consider using higher order spectral techniques as a means to generate useful features for subsequent classification by a pattern recognition engine. The core motivation for considering this approach arises from the observation that important information contained in the phase of the radar signal is lost when (second order) power spectral representations are used for feature generation. This gives rise to the exploration of higher order spectral features for this radar processing task as the phase information is retained [41]. To this end, we consider the third order spectrum, known as the bispectrum.

The bispectrum has been used as a feature vector to classify one-dimensional shapes [42] and to detect and classify buried landmines with two-dimensional GPR data [39]. This paper presents a new technique to detect the presence of an interface close to the earth's surface using bispectral features of one-dimensional GPR data.

The bispectrum $B(f_1,f_2)$ of the GPR discrete-time sequence, *x(n)*, is defined as

$$B(f_1, f_2) = X(f_1)X(f_2)X^*(f_1 + f_2) \tag{6}$$

where *X(f)* is the discrete-time Fourier transform of *x(n)*, *f* is frequency normalized by one half the sampling rate and $^*$ is the complex conjugate operator. Due to symmetry, the bispectrum is defined in the triangular region, $0 \le f_2 \le f_1 \le f_1 + f_2 \le 1$, provided there is no bispectral aliasing [42].

To obtain a feature that is more immune to noise and robust to small frequency changes in the GPR system than the power spectrum, the bispectrum is integrated [42]

$$I(a) = I_r(a) + jI_i(a) = \int_{f_1=0^+}^{1/(1+a)} B(f_1, af_1)df_1 \tag{7}$$

for $0 < a \le 1$, and $j = \sqrt{-1}$. The bispectrum is integrated along lines with slope *a* as shown in Figure 2. To obtain the feature values of the parameter, the values of *a* are chosen to be evenly spread between 0 and 1. If only one feature value is required, *a* is chosen as 1.

The bispectral-based features selected for this pattern recognition task are the magnitude and phase of the integrated bispectrum, of which the phase has useful invariant properties. These useful properties are translation invariance, dc-level, amplification, and scale invariance [42]. Even though these bispectral-based features cannot be associated with any physical electromagnetic scattering phenomena, the features represent signal shape information in a useful way offering discrimination between certain classes. The magnitude is computed as the absolute value of *I(a)* and the phase is computed using

$$P(a) = \angle I(a) = \arctan\left(\frac{I_i(a)}{I_r(a)}\right) \tag{8}$$

In practice, the value of *a* which provides the most discrimination between the classes is the best choice for a single feature. If multiple features are used (including the use of both magnitude and phase), the problem of choosing the optimal combination requires an effective discrimination measure or error statistics on data used to determine this. In this work an examination of the bispectrum and its variations on the bifrequency plane for the different classes was used to choose $a$ = 1. However, for most data there may not be significant difference in results obtained for other values of $a$ less than 1.

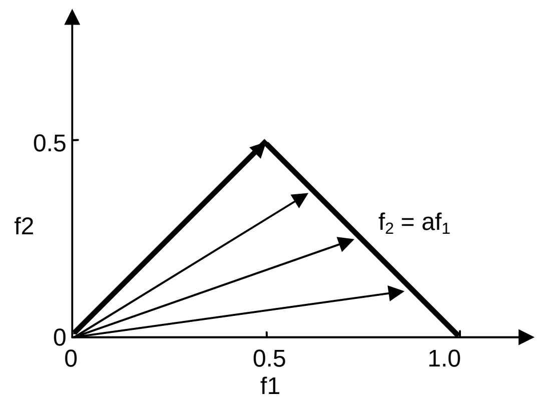


**Figure 2.** The bispectrum is integrated along lines with slope *a* chosen to be spread evenly between 0 and 1. When four parameters are computed, the values for *a* are 0.25, 0.5, 0.75, and 1.

### 2.6 Neural Network Classifier

Artificial neural networks (ANN) have become an effective classification tool in recent years [43]. One of the most common neural network architectures is the feed-forward back-propagation having an input layer, one or more hidden layers and an output layer. The number of input units is dictated by the dimensionality of the feature vector. The number of outputs is set to the number of classes in the classification model. The exception to this rule is the two class problem which can be implemented with one unit in the output layer and target labels of -1 and 1. The number of units in the hidden layer governs the complexity of the decision boundary [30] and is generally chosen empirically. The units are connected with weights that are modified during the training process. The neural network structure used in this study is shown in Figure 3.

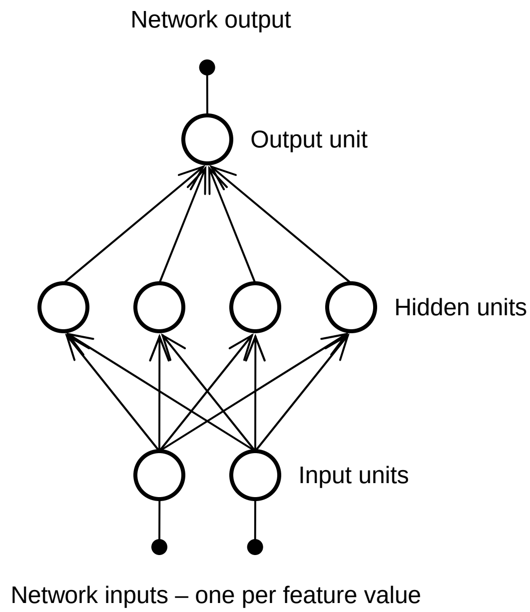


**Figure 3.** The neural network architecture used for classification.

## 3. The Experiment

### 3.1 GPR System Hardware

The laboratory experiments were conducted at CSIRO's Queensland Centre for Advanced Technologies (QCAT) in Brisbane, Australia. The system used for the experiments is a low power impulse GPR custom built by CSIRO specifically for coal related applications [44]. It has a pulse duration of 1-2 ns, dynamic range > 50 dB, equivalent time sampling rate of 111.3 GHz, and has been adapted for operation in underground coal mines. The bi-static antenna module consists of two shielded bow-tie antennas on a dielectric half space. The transmit and receive antennas have a separation distance of 5 cm and centre frequency of 1.4 GHz in air with bandwidth of 1.1 GHz. The flare angle of the bow-tie antennas is 90˚ and the maximum dimension is 7 cm resulting in a near-field far-field threshold of 6 cm [45]. A 12-bit PCMCIA data acquisition card is used to sample the data of the GPR system for processing. A typical raw waveform from this GPR in free-space is shown in Figure 4.

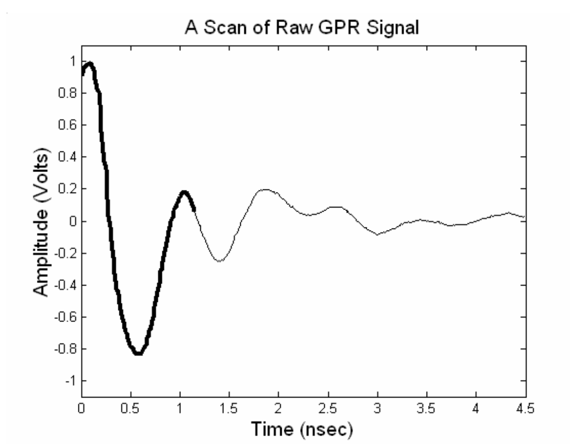


**Figure 4.** Typical raw signal obtained using the GPR system in free-space. The first segment of this signal consists of the antenna crosstalk and ringing. The thick line represents the segment used for bispectral feature extraction.

### 3.2 Experimental Testbed

A testbed was constructed so the processing can be applied to real GPR data acquired from media similar to that found in an underground coal mine. The testbed has dimensions of 2.4 × 2.25 × 0.8 m deep and the frame is timber. The testbed size was selected from standard timber sizes and the depth was chosen such that the floor is out of range of the GPR system. The horizontal layout was divided into 15 regions (see Figures 5 and 6 for a plan view and side profile respectively), where each region has either two or three layers. The bottom layer in all regions consists of wet clay with volumetric water content of 15%. The top layer for all regions accept 1 and 5 is crushed coal representing the high quality coal which would be extracted during the mining process. Regions 1 to 4 and 11 to 15 have a thin layer of shale between the bottom clay layer and top coal layer, which represents the low quality coal layer. The top layer for regions 1 and 5 is shale and clay respectively, representing the case when the coal layer has been mined right down to the surrounding strata. As it is impractical to obtain high quality coal and low quality coal, the crushed coal and shale were considered reasonable substitutes and they were readily available from a local quarry.

In the current investigation, the interface depth threshold defined at which the mining machine must retreat is 5 cm, hence regions 2 and 6 have coal layer thicknesses less than this threshold. All layers were separated by thin plastic sheets to prevent evaporation and keep the volumetric water content constant over time.

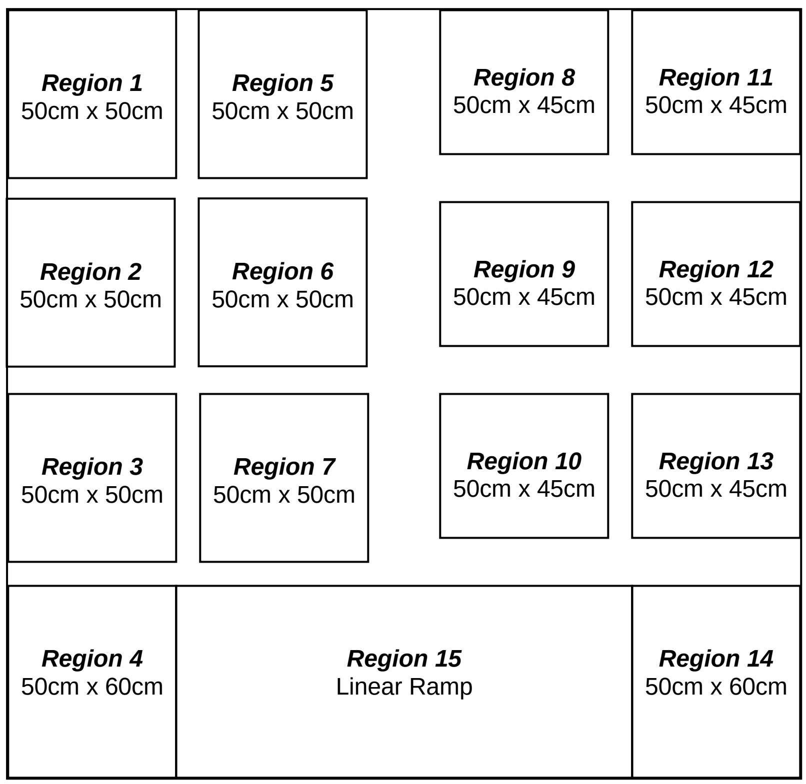


**Figure 5.** Plan view of the GPR testbed. The testbed has 14 stepped regions and a linear ramp. The layers consist of coal, shale and clay of varying thickness. The bottom layer in all regions is clay. There is no shale in regions 5 to 10 as these are for investigating coal-clay interfaces.

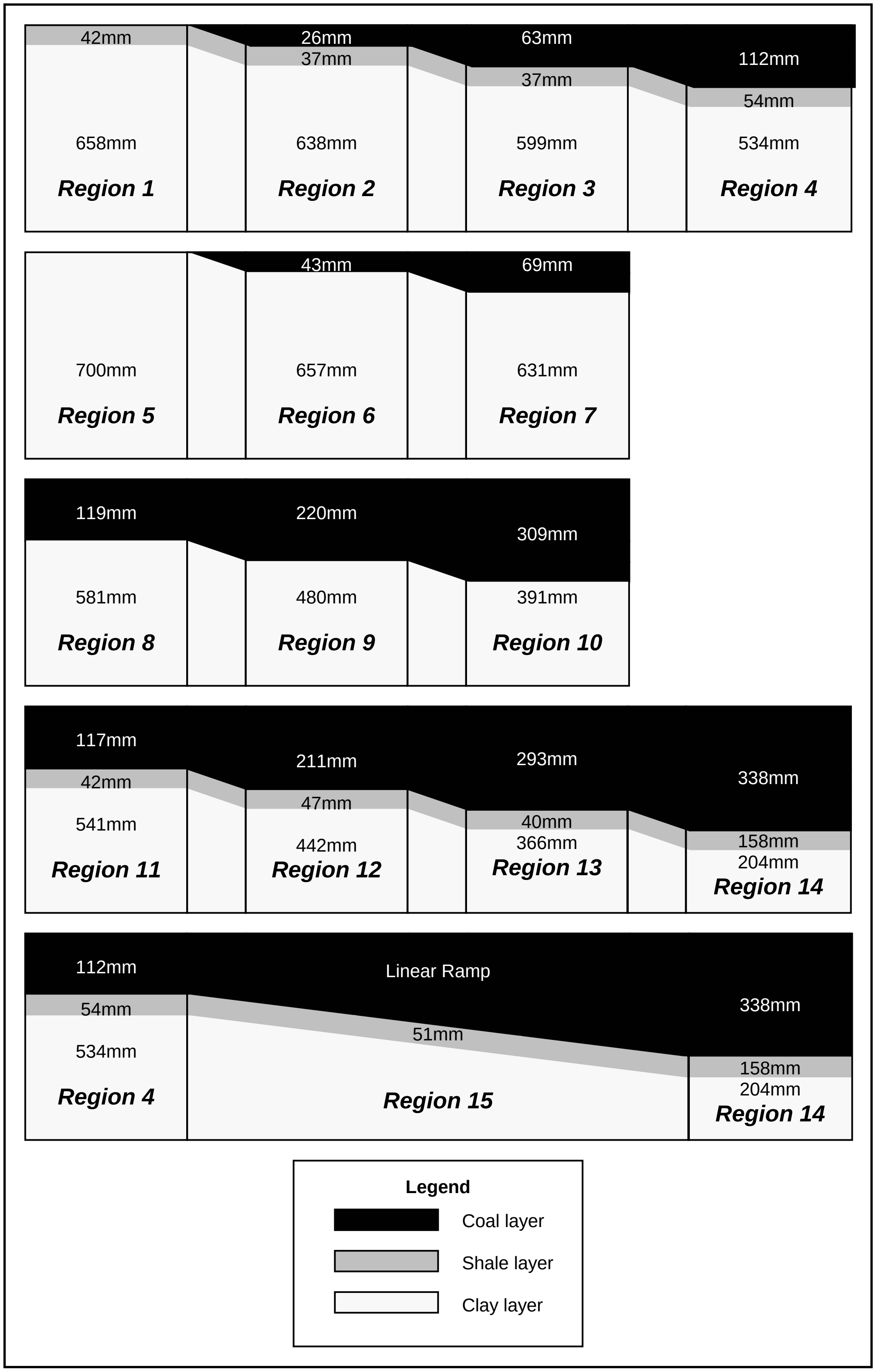


**Figure 6.** Side profile of the layers for all regions of the GPR testbed. The values shown correspond to the average thicknesses for a given region as per Table 1. The black shading represents the coal layer, the grey shading represents the shale layer and the white shading represents the clay layer.

The ground truth layer thicknesses were obtained by measuring the interface profiles for each layer during construction. Measurements were taken at spatial intervals of 20 cm intervals in both $x$ and $y$ directions and at region boundary corners using a tape measure with 1 mm resolution, as shown in Figure 7. The coal layer thickness range is 0 to 37 cm while the shale layer thickness varies between 2 and 7 cm in the shallow sections and up to 19 cm in the deepest section (region 14). Refer to Table 1 for the coal and shale layer thickness and tolerances for each region. The tolerance measurements were calculated from the measured thicknesses/depths for each region with 95% confidence covering 90% of each region surface [46].

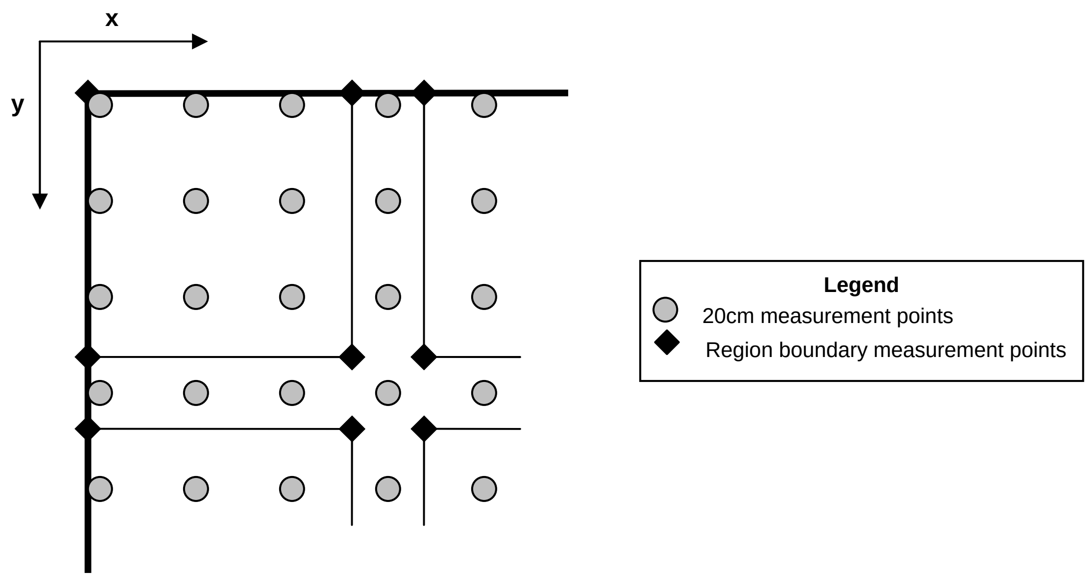


**Figure 7.** Plan view of the GPR testbed detailing the ground truth measurement points. Region 1 is shown in the top left along with the adjacent regions. The circles denote measurement points 20 cm apart whereas the diamonds represent the region boundary corners. Depth measurements of all the testbed layers and regions were taken at these points during the construction phase of the testbed.

**Table 1. Measured Testbed Layer Thicknesses**

| Region | Coal Thickness | Shale Thickness | Clay Interface Depth |
|---|---|---|---|
| 1 | No coal | 42 ± 21 mm | 42 ± 21 mm |
| 2 | 26 ± 22 mm | 37 ± 22 mm | 62 ± 9 mm |
| 3 | 63 ± 23 mm | 37 ± 21 mm | 101 ± 26 mm |
| 4 | 112 ± 31 mm | 54 ± 56 mm | 166 ± 34 mm |
| 5 | No coal | No shale | 0 mm |
| 6 | 43 ± 13 mm | No shale | 43 ± 13 mm |
| 7 | 69 ± 21 mm | No shale | 69 ± 21 mm |
| 8 | 119 ± 18 mm | No shale | 119 ± 18 mm |
| 9 | 220 ± 26 mm | No shale | 220 ± 26 mm |
| 10 | 309 ± 21 mm | No shale | 309 ± 21 mm |
| 11 | 117 ± 14 mm | 42 ± 36 mm | 159 ± 31 mm |
| 12 | 211 ± 36 mm | 47 ± 14 mm | 258 ± 29 mm |
| 13 | 293 ± 65 mm | 40 ± 62 mm | 334 ± 44 mm |
| 14 | 338 ± 45 mm | 158 ± 54 mm | 496 ± 27 mm |
| 15 | Varying | 51 ± 61 mm | Varying |

The real and imaginary dielectric constant components of the coal, shale and clay were measured using an HP8752A network analyzer with an open-ended coaxial surface probe. The frequency range measured was 100 MHz to 3 GHz. The minimum, maximum and average (in brackets) values over the antenna bandwidth for the real relative permittivity ($\varepsilon_r$'), imaginary relative permittivity ($\varepsilon_r$"), loss tangent (tanδ) and conductivity (σ) in mS/m are shown in Table 2. The average values over the full measured range are shown in Figure 8.

**Table 2. Measured Electrical Parameters of the Testbed Layers**

| Parameter | Coal | Shale | Clay |
|---|---|---|---|
| $\varepsilon_r$' (avg) | 3.8-5.3 (4.4) | 3.1-12.7 (9.1) | 22.7-27.2 (24.9) |
| $\varepsilon_r$" (avg) | 0.1 – 0.5 (0.26) | 0.2 – 4.5 (2.1) | 5.2 – 9.9 (6.9) |
| tanδ (avg) | 0.02 – 0.1 (0.05) | 0.1 – 0.4 (0.2) | 0.2 – 0.4 (0.3) |
| σ - mS/m (avg) | 14.3 – 25.6 (20.5) | 133.1 – 176.4 (154.6) | 438.6 – 602.1 (517.6) |

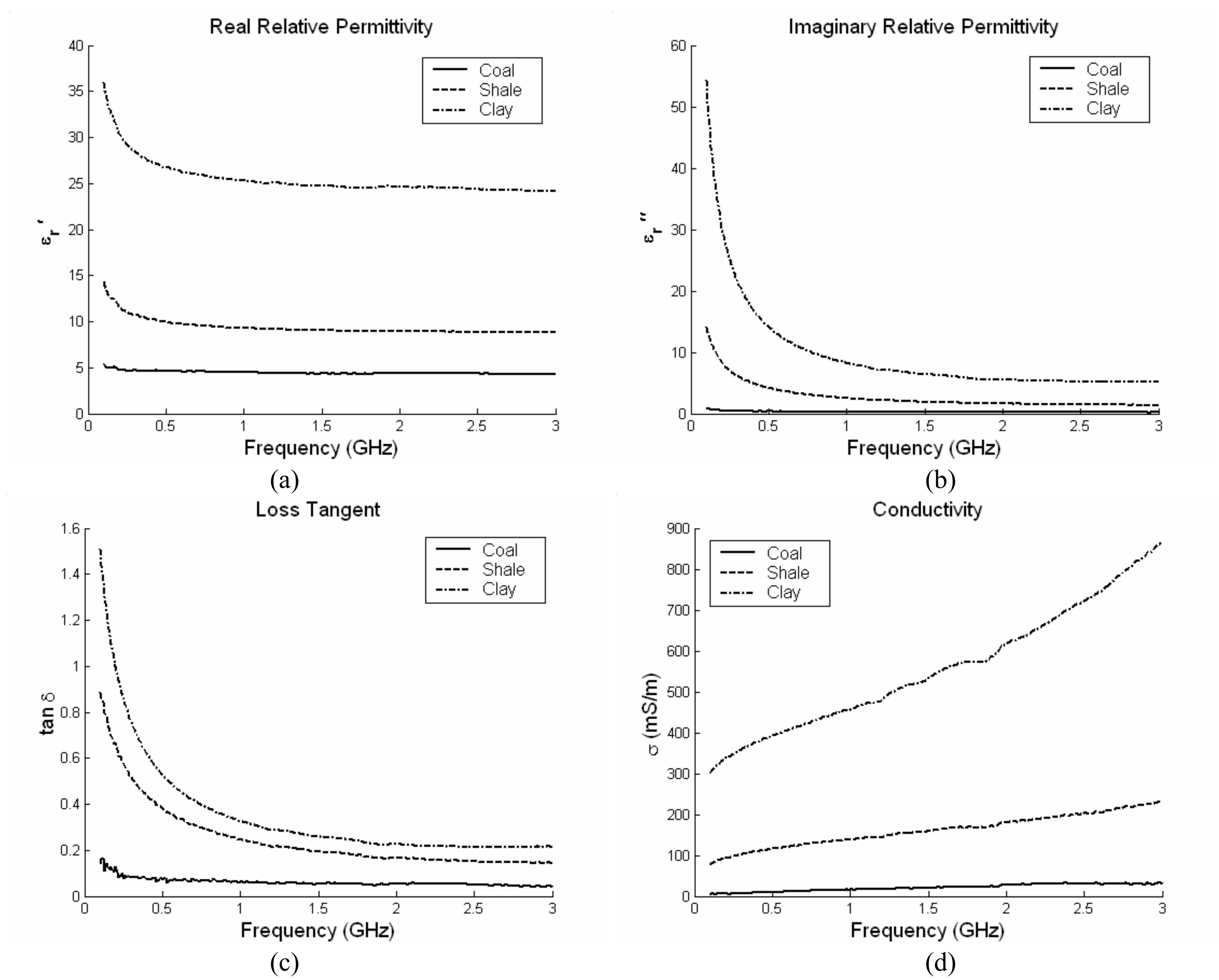


**Figure 8.** Measured electrical parameters of coal, shale and clay of GPR testbed from 100 MHz to 3 GHz. The parameters shown are (a) real relative permittivity ($\varepsilon_r$'), (b) imaginary relative permittivity ($\varepsilon_r$"), (c) loss tangent (tanδ), and (d) conductivity (σ) in mS/m.

### 3.3 Processing

Three signal processing techniques were implemented for the near-surface interface detection task. The first two were pattern recognition approaches and the third was the matched filter as a time delay estimator. The feature vector for the first pattern recognition approach was the magnitude and phase of the integrated bispectrum. For the second approach, the feature vector consisted of parameters extracted from the power spectrum. The final stage of the two pattern recognition systems utilized a neural network classifier. The implementation of these pattern recognition approaches and the matched filter is explained in this section.

The first stage of any pattern recognition system is data pre-processing. The pre-processing implemented for both pattern recognition approaches were DC offset removal and sum of squares normalization. Note that no background or ground clutter subtraction routines were utilized for these pattern recognition systems.

The processing for extraction of the integrated bispectrum feature vector included truncating the pre-processed GPR data to the first 128 samples, windowing the truncated data with a Hamming window, computation of the integrated bispectrum and phase unwrapping to eliminate jumps over $2\pi$ radians. The parameter $a$ of the integrated bispectrum was chosen as 1 as just one pair of features provided suitable discrimination.

Similarly, the power spectrum feature extraction stage included truncating the pre-processed data to the first 128 samples. The power spectrum was estimated using the modified periodogram utilizing the 128 point fast Fourier transform (FFT) with a Hamming window. The Hamming window provides a good tradeoff between mainlobe resolution and sidelobe attenuation [47]. The second and third points of the resulting modified periodogram provided sufficient discrimination and hence were chosen as the feature vector for the power spectrum based pattern recognition approach.

The neural network structure used for classifying the integrated bispectrum and power spectrum feature vectors was the fully-connected three layer feed-forward architecture with two and four units in the input and hidden layers respectively. As the application has been cast as a two category classification problem, one unit was selected for the output layer. The activation function type was hyperbolic tangent sigmoid for the hidden layer and pure linear for the output layer.

Prior to network training, the mean and variance of the training data feature vectors were estimated. These estimates were used to standardize both the training and test data so that each feature input to the neural network was zero mean with a variance of one. This ensures each feature has equal weight during the classification stage [30]. The networks were trained using the back-propagation learning algorithm with data from regions 2 and 6 for the *coal thickness less than 5 cm* class, and data from regions 3, 4, 7, and 8 for the *coal thickness greater than 5 cm* class. The training data was acquired with the antenna module positioned in the centre of each corresponding region. As the testing and training data must not be the same, the data used to test the pattern recognition systems was acquired while the antenna module was being moved over the region of interest. The category labels used during training were 1 and -1 for the *coal thickness less than 5 cm* and *coal thickness greater than 5 cm* classes respectively.

The matched filter cannot be implemented to detect the near-surface interface as elegantly as the pattern recognition approaches in this study. Hence, the motivation behind using the matched filter was one of time delay estimation as opposed to signal detection. The peak of the likelihood ratio function (1) is used to estimate the time delay of a target reflection. The time of the likelihood ratio function peak corresponds to the point of highest correlation between the signal and transmitted signal estimate. The interface depth is then estimated using (2) and (3) from knowledge of the relative permittivity of the coal. The estimate of the transmitted signal was obtained from a flat metal plate scan after subtraction of a free space calibration signal. The metal plate was 40cm from the antenna module to ensure that the corresponding reflection was not masked by the antenna ringing.

The pre-processing stages implemented for the matched filter were background subtraction and an exponential time-varying gain function as in [48]. The relative permittivity of the coal layer for the propagation velocity estimate was taken as 4.4 as given in Table 2. To allow a performance comparison between the matched filter and the pattern recognition approaches, the processed output is classified into the *coal thickness less than 5 cm* and *coal thickness greater than 5 cm* classes directly from the interface depth estimate.

## 4. Discussion of Results

The experimental results were classified into two classes according to the coal layer thickness (coal-shale and coal-clay interface depths) as less than 5 cm and greater than 5 cm with a tolerance of 0.5 cm. The significance of these classes is related to what action the mining machine should take. If the coal layer thickness is less than 5 cm, the optimal amount of extracted coal has been reached and the miner should retreat. Conversely, if the coal layer thickness is greater than 5 cm, more coal can be mined.

Figure 9 shows the integrated bispectral magnitude versus phase feature values for the *coal thickness less than 5 cm* and *coal thickness greater than 5 cm* classes for the coal-clay and coal-shale interfaces. The data for the coal-clay interface was acquired from regions 5 to 10 while the data for the coal-shale interface was from regions 1 to 4 and 11 to 14. The regions from which the data for each cluster were acquired are shown in Table 3. The antenna module was moved around the corresponding region during data acquisition. As a result, the feature values within the clusters are spread due to varying interface depths and the inhomogeneous layers.

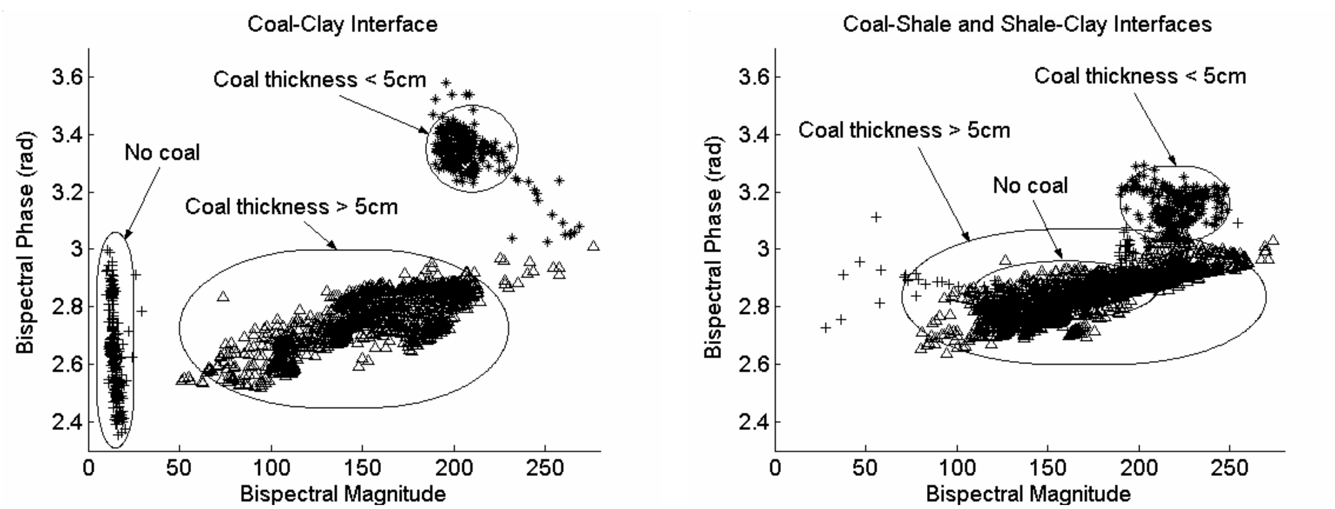


(a) (b)

**Figure 9.** The bispectral magnitude and phase feature values for varying coal layer thicknesses with (a) coal-clay, (b) coal-shale and shale-clay interfaces. The clusters for no coal, coal thickness less than 5 cm and greater than 5 cm have been circled.

**Table 3. GPR Testbed Regions in Feature Clusters**

| Cluster | Coal-Clay Regions | Coal-Shale Regions |
|---|---|---|
| No coal | 5 | 1 |
| Coal thickness < 5 cm | 6 | 2 |
| Coal thickness > 5 cm | 7, 8, 9, 10 | 3, 4, 11, 12, 13, 14 |

Energy reflected from an interface near the surface modifies the early time signal of the data and hence the features in a deterministic but unknown manner. The effect on the early time signal is more evident for the coal-clay interface than the coal-shale interface because the relative permittivity and conductivity contrast between the coal and clay is much greater than the coal and shale as seen in Figure 8 and Table 2. Hence, the *coal thickness less than 5 cm* cluster is well separated from the *coal thickness greater than 5 cm* cluster for the coal-clay interface as opposed to the same classes for the coal-shale interface (refer to Figures 9 (a) and (b)).

The data obtained for the *coal thickness less than 5 cm* cluster in Figure 9 (b) was for region 2. In addition to the coal-shale interface at 26 ± 22 mm, this region has a shale-clay interface at a total depth of 62 ± 9 mm (from Table 1) which is greater than 5 cm. If the reflection from the shale-clay interface is similar or greater in magnitude than the reflection from the coal-shale interface, this would affect the feature values by shifting them towards the cluster of the more dominant component.

The large cluster for the *coal thickness greater than 5 cm* class in Figures 9 (a) and (b) represent feature values for multiple regions (refer to Table 3). The mapping between the feature values and the interface depth is not a linear one. Therefore it is possible for a cluster corresponding to a region to be in between two other clusters even though their interface depths are not sequential.

The neural network classifier output is a number between -1 and 1 representing the *coal thickness greater than 5 cm* and *coal thickness less than 5 cm* classes respectively. The output of the matched filter is the interface depth estimate in centimeters. The logical choice for a simple threshold to separate the two classes is 0 for the pattern recognition approaches and 5 for the matched filter depth estimator. The detection and false alarm rates using these thresholds are shown in Table 4.

**Table 4. Detection and False Alarm Rates**

| Feature Vector | Coal-Clay Regions | | Coal-Shale Regions | |
|---|---|---|---|---|
| | Detection Rate (%) | False Alarm Rate (%) | Detection Rate (%) | False Alarm Rate (%) |
| Integrated Bispectrum | 94.7 | 0.1 | 84.1 | 1.8 |
| Power Spectrum | 80.4 | 0 | 38.0 | 0 |
| Matched Filter | 89.3 | 0.2 | 62.3 | 12.0 |

The desired performance of a detector is sometimes specified with either constant detection or false alarm rates and is usually application specific. This simplistic approach to threshold determination does not always yield optimal performance. The detector can be optimized by changing the threshold to minimize detection errors. The detection error tradeoff (DET) curve is a useful means to compare detection schemes. The DET curves for the classifiers using the integrated bispectrum, power spectrum and matched filter for the coal-shale interface are shown in Figure 10. This presents the change in detection error as the thresholds are varied.

The high false alarm rate for the matched filter at the stepped point in Figure 10 (miss rate ≈ $10^{-2}$) is due to the residual error from the background (antenna ringing and crosstalk) subtraction pre-processing stage and the inhomogeneous layers. The pattern recognition based processing does not rely on subtracting the antenna ringing or crosstalk, rather subtle changes in the signal less dominant than the ringing maintain the clusters in close proximity to the no target present case, yet provides sufficient power for detection. It can be seen that bispectral features provide better performance over the power spectrum and matched filter for detecting near-surface interfaces for this coal mining application. The magnitude and phase of the integrated bispectrum are thus valid features for the near-surface interface detection problem. The DET curves for the coal-clay interface are not shown because the clusters are well separated as in Figure 9(a). The classifier has a simple task when given such well separated features as seen in the low false alarm rates in Table 4.

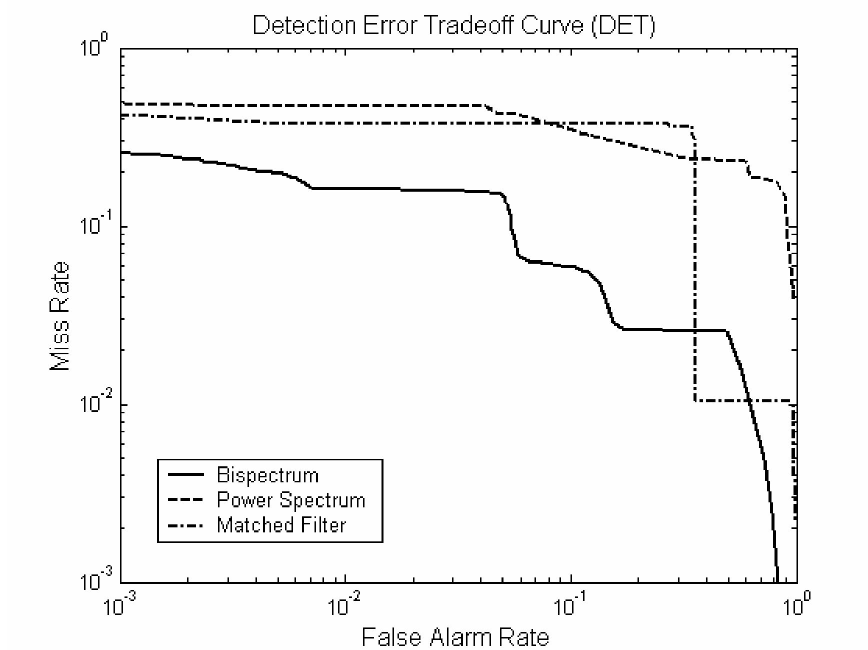


**Figure 10.** Detection error tradeoff (DET) curves for the bispectral features, power spectrum and the matched filter for the coal-shale interface.

## 5. Conclusion

The detection of coal seams close to the ground surface is a problem that has not yet been satisfactorily solved. This paper considered the use of GPR as the primary sensor for this task. Whilst GPR offers considerable promise for this problem, it also raises a number of practical processing issues which cannot all be reliably addressed using traditional processing techniques. As a consequence, new methods were implemented and compared with the classical approaches for the near-surface interface detection task. The first two pattern recognition approaches utilized an artificial neural network to classify features based on the bispectrum and the power spectrum. The third approach was a matched filter based time delay estimator. A comparative analysis has shown that the magnitude and phase of the integrated bispectrum are useful features in detecting the presence of near-surface interfaces. Real GPR data was obtained from a testbed constructed with coal-shale, coal-clay and shale-clay interfaces representing returns from a coal mining environment. The detection task was divided into two classes, namely *coal layer thickness less than 5 cm* and *coal layer thickness greater than 5 cm*. The feature vector that provided the best result was the real and imaginary components of the integrated bispectrum. The results obtained here highlight the efficacy and benefits of a neural-network approach as a solution to this problem. In this paper, we are not addressing the problem of depth estimation, rather confining ourselves to detecting an interface within a particular depth range. The complementary depth estimation task will need to consider the non-linear relationship between the features and depth.

## 6. Acknowledgement

The authors would like to kindly thank the members of the CSIRO Mine Automation Group, Queensland, Australia for the use of their facilities, GPR system, and data. The authors would also like to thank Mr. Andrew Castleden of the CSIRO for his work in the design and construction of the GPR testing facilities, and Mr. Mark Kochanek of the CSIRO for assisting with the dielectric measurements.

## 7. References


1. Ralston, J.C. and Hainsworth, D.W., 1999, Application of ground penetrating radar for coal depth measurement: IEEE International Conference on Acoustics, Speech and Signal Processing (ICASSP99), p. 2275-2278.

2. Stolarczyk, L.G. and Stolarczyk, G.L., 1998, Electromagnetic wave detection and imaging technologies (EDIT) for reducing ash, sulfur, and heavy metals in run-of-mine coal: Proceedings (CD-ROM) of the 15th Annual International Pittsburgh Coal Conference, Pittsburgh, USA.

3. Ralston, J.C., Hainsworth, D.W., Reid, D.C., Anderson, D.L., and McPhee, R.J., 2001, Recent advances in remote coal mining machine sensing, guidance, and teleoperation: Robotica, v. 19, p. 513-526.

4. Stolar Horizon Inc., 2002, Stolar Horizon, Inc., Installs Breakthrough Horizon Sensing Technology, (http://www.stolarhorizon.com/press-release.htm).

5. Daniels, D.J., Gunton, D.J., and Scott, H.F., 1988, Introduction to subsurface radar: IEE Proceedings Pt. F, v. 135, p. 278-320.

6. Peters Jr., L.P., Daniels, J.J., and Young, J.D., 1994, Ground penetrating radar as a subsurface environmental sensing tool: Proc. of the IEEE, v. 82, p. 1802-1822.

7. Ellerbruch, D.A., and Belsher, D.R., 1978, Electromagnetic technique of measuring coal layer thickness: IEEE Transactions on Geoscience and Remote Sensing, v. GE-16, pp. 126-133.

8. Noon, D. A., 1996, Stepped-frequency radar design and signal processing enhances ground penetrating radar performance: PhD thesis, Department of Electrical & Computer Engineering, University of Queensland and Cooperative Research Centre for Sensor Signal and Information Processing.

9. Daniels, D.J., 1980, Short pulse radar for stratified lossy dielectric layer measurement: IEE Proceedings Pt. F, v. 127, p. 384-388.

10. Chufo, R.L., and Johnson, W.J., 1993, A radar coal thickness sensor: IEEE Transactions on Industry Applications, v. 29, no. 5, p. 834-840.

11. Mowrey, G.L., Ganoe, C.W., and Monaghan, W.D., 1997, A radar-based highwall rib-thickness monitoring system: Fuel and Energy Abstracts, v. 38, p. 194-198.

12. Yelf, R.J., 1996, Ground penetrating radar in open pit coal mines for mapping of overburden, seam thickness and guidance of continuous mining machines: Proceedings of the 6th International Conference on Ground Penetrating Radar (GPR 96), p. 113-116.

13. Jha, P.C., Balasubramaniam, V.R., Sandeep, N., Sivaram, Y.V., and Gupta, R.N., 2004, GPR applications in mapping barrier thickness in coal mines: Some case studies: Proceedings (CD-ROM) of the 10th International Conference on Ground Penetrating Radar (GPR 2004), Delft, Netherlands.

14. Hainsworth, D.W., McPhee, R.J., and Ralston, J.C., 1999, Longwall horizon control (ACARP project C4018): CSIRO Exploration and Mining Report 658F, Kenmore, QLD, Australia.

15. Murray, W., Williams, C., Pollock, J. T. A., Hatherly, P., and Hainsworth, D., 1996, Ground probing radar applications in the coal industry: Proceedings of the 6th International Conference on Ground Penetrating Radar (GPR 96), p. 107-112.

16. Strange, A.D., Chandran V. and Ralston, J.C., 2004, Subsurface interface detection using bispectral features and ground penetrating radar: Proceedings of the IASTED International Conference on Antennas, Radar, and Wave Propagation, Banff, Canada, p. 191-196.

17. Maser, K.R., 2003, Non-destructive measurement of pavement layer thickness: Final Report – Caltrans No. 65A0074.

18. Roberts, R.L., and Petroy, D., 1996, Semi-automatic processing of GPR data collected over pavements: Proceedings of the 6th International Conference on Ground Penetrating Radar (GPR 96), p. 347-352.

19. Spagnolini, U. and Rampa, V., 1999, Multitarget detection/tracking for monostatic ground penetrating radar: application to pavement profiling: IEEE Transactions on Geoscience and Remote Sensing, v. 37, p. 383-394.

20. Saarenketo, T., and Scullion, T., 2000, Road evaluation with ground penetrating radar: Journal of Applied Geophysics, v. 43, Issues 2-4, p. 119-138.

21. Lambot, S., Slob, E.C., van den Bosch, I., Stockbroeckx, B., and Vanclooster, M., 2004, Modeling of ground-penetrating radar for accurate characterization of subsurface electric properties: IEEE Transactions on Geoscience and Remote Sensing, v. 42, no. 11, p. 2555-2568.

22. Lazaro-Mancilla, O., and Gomez-Trevino, E., 2000, Ground penetrating radar inversion in 1-D: an approach for the estimation of electrical conductivity, dielectric permittivity and magnetic permeability: Journal of Applied Geophysics, v. 43, Issues 2-4, p. 199-213.

23. van der Merwe, A., and Gupta, I.J., 2000, A novel signal processing technique for clutter reduction in GPR measurements of small, shallow land mines: IEEE Trans. Geosc. and Remote Sensing, v. 38, no. 6, p. 2627-2637.

24. van Kempen, L., Sahli, H., Brooks, J., and Cornelis, J., 2000, New results on clutter reduction and parameter estimation for landmine detection using GPR: Proceedings of the 8th International Conference on Ground Penetrating Radar (GPR 2000), p. 872-879.

25. Sai, B., and Ligthart, L.P., 2003, Effective clutter removal for detecting non-metallic mines in various soil fields: Proceedings of the IEEE Intl Geoscience and Remote Sensing Symp (IGARSS '03), v. 2, p. 764-766.

26. Abujarad, F., Jöstingmeier, A., and Omar, A.S., 2004, Clutter removal for landmine using different signal processing techniques: Proceedings (CD-ROM) of the 10th International Conference on Ground Penetrating Radar (GPR 2004), Delft, Netherlands.

27. Flores-Tapia, D., Thomas, G., and Phelan, M.C., 2004, Clutter reduction of GPR images using multiscale products: Proceedings of the IASTED International Conference on Antennas, Radar, and Wave Propagation, Banff, Canada, p. 181-185.

28. Ebihara, S., 2003, Blind separation for estimation of near-surface interface by GPR with time-frequency distribution: IEICE Transactions on Communications, v. E86-B, no. 10, p. 3071-3081.

29. Kay, S. M., 1998, Fundamentals of Statistical Signal Processing: Detection Theory, Prentice Hall PTR, Upper Saddle River, New Jersey.

30. Duda, R.O., Hart, P.E., Stork, D.G., 2001, Pattern Classification, 2nd ed., John Wiley & Sons, New York, NY.

31. Chan, L.C., Moffatt, D.L., and Peters, L., 1979, A characterization of sub-surface radar targets: Proc. of the IEEE, v. 67, p. 991-1000.

32. Carevic, D., 1998, An approach to characterizing ground probing radar target echoes for landmine recognition: Technical Report DSTO-TR-0680, DSTO, Salisbury, Australia.

33. Carevic, D., Chant, I., and Caelli, T., 1999, Feature extraction and classification of minelike targets from GPR data using Gaussian mixture models: Proc. Information, Decision and Control (IDC 99), p. 329-334.

34. Al-Nuaimy, W., Huang, Y., Nakhkash, M., Fang, M.T.C., Nguyen, V.T., and Eriksen, A., 2000, Automatic detection of buried utilities and solid objects with GPR using neural networks and pattern recognition: Journal of Applied Geophysics, v. 43, Issues 2-4, 157-165.

35. Gamba, P. and Lossani, S., 2000, Neural detection of pipe signatures in ground penetrating radar images: IEEE Transactions on Geoscience and Remote Sensing, v. 38, no. 2, p. 790-797.

36. Youn, H.S., and Chen, C.C., 2004, Neural detection for buried pipe using fully polarimetric GPR: Proceedings (CD-ROM) of the 10$^{th}$ International Conference on Ground Penetrating Radar (GPR 2004), Delft, Netherlands.

37. Newnham, L., and Goodier, A., 2000, Using neural networks to interpret sub-surface radar imagery of reinforced concrete: Proceedings of the 8$^{th}$ International Conference on Ground Penetrating Radar (GPR 2000), p. 434-440.

38. Deming, R.W., 1998, Automatic buried mine detection using the maximum likelihood adaptive neural system (MLANS): Proceedings of the 1988 IEEE International Symposium on Intelligent Control (ISIC), p. 428-433.

39. Balan, A,N, and Azimi-Sadjadi,, M.R., 1995, Detection and classification of buried dielectric anomalies by means of the bispectrum method and neural networks: IEEE Transactions on Instrumentation and Measurement, v. 44, p. 998-1002.

40. Oppenheim, A. V., Schafer, R. W., and Buck, J. R., 1999, Discrete-time signal processing, 2$^{nd}$ ed., Prentice-Hall, Inc., Upper Saddle River, New Jersey.

41. Nikias, C.L., and Petropulu, A.P., 1993, Higher-order spectra analysis, a nonlinear signal processing framework, PTR Prentice Hall, Englewood Cliffs, NJ.

42. Chandran, V., and Elgar, S.L., 1993, Pattern recognition using invariants defined from higher order spectra – one-dimensional inputs: IEEE Transactions on Signal Processing, v. 41, p. 205-212.

43. Chakrabarti, S., Bindal, N., and Theagharajan, K., 1995, Robust radar target classifier using artificial neural networks: IEEE Transactions on Neural Networks, v. 6, no. 3, p. 760-766.

44. Murray, W., Lewis, C., Yang, Z., and Pollock, J., 1996, Development of high resolution GPR hardware in the frequency range 300 MHz - 3.5 GHz: Proceedings of the 6$^{th}$ International Conference on Ground Penetrating Radar (GPR 96), p. 505-510.

45. Sadiku, M.N.O., 1995, Elements of Electromagnetics, 2$^{nd}$ ed., Oxford University Press, New York, NY.

46. Hogg, R.V., Ledolter, J., 1987, Engineering Statistics, Macmillan Publishing Company, New York, NY.

47. Hayes, M.H., 1996, Statistical Digital Signal Processing and Modeling, John Wiley & Sons, New York, NY.

48. Strange, A.D., Chandran V. and Ralston, J.C., 2002, Signal processing to improve target detection using ground penetrating radar: Proceedings of the 4$^{th}$ Australasian Workshop on Signal Processing and Applications (WoSPA 2002), p. 139-142.